Supporting Online Material for

Interfacial Polygonal Nanopatterning of Stable Microbubbles

Emilie Dressaire, Rodney Bee, David C. Bell, Alex Lips, Howard A. Stone*

*To whom correspondence should be addressed. E-mail: has@seas.harvard.edu

Published 30 May 2008, *Science* **320**, 1198 (2008)
DOI: 10.1126/science.1154601

This PDF file includes:

Interfacial polygonal nanopatterning of stable microbubbles

Supporting Online Material

Emilie Dressaire[1], Rodney Bee[2], David C. Bell[1],

Alex Lips[2], and Howard A. Stone[1,*]

[1] *School of Engineering and Applied Sciences, Harvard University, Cambridge, Massachusetts 02138, USA*

[2] *Unilever Research & Development, 40 Merritt Boulevard, Trumbull, Connecticut 06611, USA*

**To whom correspondence should be addressed;*

E-mail: has@seas.harvard.edu.

Supporting Online Material:

Materials and Methods

Dispersion preparation

The sample is prepared by mixing 187.5 g of glucose syrup (75% wt. %, Cargill ClearSweet 63/43 Corn syrup), 5 g of a mixture of sucrose esters (2 wt. %, S1670, Mitsubishi Food Corporation) and 57.5 g of water. The surfactant mixture contains mostly sucrose mono- and di-ester and less than 3% of tri-ester (*S1*). The surfactant molecules are first dissolved in water by heating to 70°C. The glucose syrup is heated to 70°C separately. Both constituents are mixed and poured in a mixer (Kitchen Aid Artisan with whip paddle) where the solution is sheared for two hours. The sample cools down to room temperature during aeration. We estimate the shear rate as $\dot{\gamma} \approx a\,\Omega/h$, where a is the radius of the whip, Ω the angular velocity, and h the distance between the whip and the bowl. Aerated samples are stored at 4°C.

Microscopy techniques

Vitrified samples for Cryo-Transmission Electron Microscopy (cryo-TEM): Specimens for cryo-TEM are prepared in a controlled environment vitrification system. The samples are diluted in water (0.5 g in 10 mL), immediately before vitrification, to lower the viscosity. The stability of the microbubbles is highly sensitive to the solubility of the surfactant molecules, which increases upon dilution. The diluted samples need to be frozen immediately after preparation so that the interfacial structure of the bubble is not disrupted: the transfer of surfactant molecules from the interface to the bulk phase

could alter the hexagonal structures observed in our micrographs.

To freeze a nanometer thick layer of sample, 20 μL of diluted sample are placed on a TEM grid. The excess solution is blotted with filter paper, and the thin layer is quenched by plunging into liquid ethane at its melting point. Specimens are examined below -178°C in a JEOL 2100 microscope, operated under low dose, using a cryo-holder.

Fracture replication for Transmission Electron Microscopy (TEM): Freeze-fracture replication is performed with a BAF301 system. A small drop of sample is deposited between two gold planchettes and plunged into liquid nitrogen at its freezing point. The "sandwich" is placed in a pre-cooled sample fracture block, which, under vacuum, is split open to fracture the sample. The new surfaces are shadowed at a 45° angle with platinum (2 nm), and then at a 90° angle with carbon to form a uniform 20 nm backing layer. The replicas are floated off the samples, cleaned in bleach and distilled water, mounted on TEM grids, and examined in a JEOL 2100 TEM at room temperature.

Cryo-Scanning Electron Microscopy (Cryo-SEM): A drop of sample is placed on a stub and plunged into liquid nitrogen at its freezing point. The sample is then introduced in the cooling pre-chamber (-90ºC) and fractured with a cool knife. The surface is sputtered with gold to form a 4-8 nm thick conductive layer, which is transferred to the DB235 FIB/SEM for examination at -180ºC.

Supplementary text

Hollowness of microbubbles

The microbubble in fig. S1 is fractured along a plane above its equator during the freeze-fracture preparation and imaged with TEM. This conclusion follows from the fact that the radius of the cut section (bright area) is smaller than the radius of the bubble (larger dark circle). The platinum shadow results from the metal deposition. It covers part of the inner area of the bubble, since it is observed to shift from left to right on the different images of fig. S1 (images obtained by tilting the replica under a fixed electron beam). This observation shows that the microbubbles are hollow and are not surfactant aggregates.

Measurement of bubble radius from TEM image of replica

The radius of a microbubble can be obtained from the TEM image of its replica, assuming that the plane of fracture is flat. Using the notations of fig. S2, we denote the radius of the section of the bubble in the fracture plane as $R_d = S' + B'$ and the relative area shadowed as S'. Then, the radius of the bubble is determined using geometry:

$$R_b = \frac{S'}{\sin\left(\arctan\left(\left(\frac{S'}{S'+B'}\right)\right)\right)} \qquad \text{(s1)}$$

In the data shown in Fig. 2, only the patterns located near the center of the images of fully patterned bubbles are used to evaluate the average pattern size.

Properties of the condensed phase

Molecular composition: When characterizing aggregates of surfactant molecules, it is common to introduce the close-packing parameter defined as $\bar{v}/a_0\ell_c$, where a_0 is the surface area occupied by the headgroup of the molecule, and ℓ_c and $\bar{v}$ are, respectively, the length and the volume of the carbonyl chains (*S2*). Before aeration, lamellae of surfactant molecules form in the medium (fig. S3), which means that the close-packing parameter of the condensed phase is close to 1 (*S2*), i.e. that the average shape of the surfactant molecules is a cylinder. Here $a_0 \approx 0.3\,\text{nm}^2$ in the condensed phase (*S3*) and ℓ_c is the length of a fully extended 18-carbon chain, $\ell_c \approx 2.4\,\text{nm}$ (*S2*). Also, $\bar{v}$ depends on the composition of mono- and di-ester at the interface. The condition imposed on the close-packing parameter leads to $\bar{v} \approx 0.72\,\text{nm}^3$. The volume of a carbonyl chain in an aggregate is about 0.5 nm^3 (*S2*). We conclude that the composition of the condensed phase is approximately 59% mono-ester and 41% di-ester. The composition difference between the initial surfactant mixture and the condensed phase is due to the different solubilities and surface activities of the ester molecules, as observed experimentally in water (*S4*).

Spontaneous radius of curvature: After aeration, fewer lamellae are observed in the bulk phase, which indicates that the condensed phase of surfactant molecules now sits on the air/liquid interface. The carbonyl chains adopt a different configuration in air where they are expected to be in a frozen state, where each of them occupy a surface area s = 0.2 nm^2 (*S5*). The surfactant molecules can therefore be modeled as close-packed truncated cones (Fig. 3F). We take into account the geometrical differences between

mono- and di-ester, i.e. single versus double chains. The molecules tend to bend the interface, which adopts a radius of curvature R_{sp} on the liquid side and a slightly smaller radius R_{sp}- ℓ_c on the air side. The phase composition determined above and the geometry of the truncated cones lead to the following relation:

$$\left(\frac{R_{sp}}{R_{sp} - \ell_c} \right) = \frac{a_0}{0.59s + 0.41.2s} \qquad \text{(s2)}$$

The spontaneous radius of curvature of the condensed phase is estimated from this equation to be 80 nm. Thus, it is energetically favorable for the molecules to sit on curved interfaces with comparable radii of curvature.

Energy of the bubble and structuring of the interface

Definition of the energy: The energy of the system is defined as the sum of the energies associated with bending elasticity of the interface (bending rigidity $\kappa \approx 8.10^{-19}$ J, spontaneous radius of curvature R_{sp}), with the formation of domain boundaries (line tension $\lambda \approx 2.10^{-12}$ J.m^{-1}) and with the shrinkage of the microbubble (normal pressure-volume work, pV):

$$E(a, R_c) = n \left(A \frac{\kappa}{2} \left(\frac{2}{R_c} - \frac{2}{R_{sp}} \right)^2 + \lambda \pi a \right) - pV \qquad \text{(s3)}$$

The geometrical parameters of the domains are (Fig. 3E): their surface area A, their radius a, and the radius of curvature R_c. The surface area can now be written:

$$A = 2\pi {R_c}^2 \left(1 - \sqrt{1 - \left(\frac{a}{R_c} \right)^2} \right) \tag{s4}$$

Using the notation of Fig. 3E, the volume of the bubble is decomposed into the volume of the core (a sphere of radius R_b') and the volume of the *n* domains that buckle the interface:

$$V = V_{core} + nV_{domains} \approx V_{core} \approx \frac{4}{3}\pi {R_b}'^3 \approx \frac{4}{3}\pi \left(\frac{\sqrt{n}a}{2} \right)^3 \tag{s5}$$

The total energy *E* can be written:

$$E(a, R_c, n, \lambda, \kappa, R_{sp}, p) = n \left(4\pi\kappa R_c^2 \left(1 - \sqrt{1 - \left(\frac{a}{R_c} \right)^2} \right) \left(\frac{1}{R_c} - \frac{1}{R_{sp}} \right)^2 + \pi\lambda a \right) - \frac{\pi}{6} p \left(\sqrt{n}a \right)^3 \tag{s6}$$

Minimization under constraint: The surfactant molecules are assumed to be pinned on the interface because of their limited solubility and the formation of a condensed phase. The surface area of the buckled microbubble is therefore equal to the surface area of the initial spherical bubble of radius R_b:

$$4\pi R_b^2 = nA = 2\pi n R_c^2 \left(1 - \sqrt{1 - \left(\frac{a}{R_c} \right)^2} \right) \tag{s7}$$

The energy of the system is minimized under this assumption of fixed area. Using the method of Lagrange multipliers, we write:

$$E_1 = n\left(4\pi\kappa R_c^2\left(1-\sqrt{1-\left(\frac{a}{R_c}\right)^2}\right)\left(\frac{1}{R_c}-\frac{1}{R_{sp}}\right)^2 + \pi\lambda a\right) - \frac{\pi}{6}p\left(\sqrt{n}a\right)^3 \\ -\beta\left(2\pi n R_c^{\,2}\left(1-\sqrt{1-\left(\frac{a}{R_c}\right)^2}\right) - 4\pi R_b^{\,2}\right) \tag{s8}$$

where β is the Lagrange multiplier associated with the constraint on the surface area.

We define:

$$u = \frac{a}{R_c} \qquad v = \frac{R_c}{R_{sp}} \qquad \Lambda = \frac{\lambda R_b}{4\kappa} \qquad B = \frac{\beta R_b^2}{\kappa} \qquad C = \frac{pR_b^3}{24\kappa} \qquad r = \frac{R_{sp}}{R_b}$$

so that the energy can be non-dimensionalized:

$$E_2(n,u,v,\beta) = \frac{E_1}{4\pi\kappa} = n\left(1-\sqrt{1-u^2}\right)(1-v)^2 + \Lambda n r u v - C n^{3/2}(ruv)^3 \\ -B\left(\frac{nr^2}{2}v^2\left(1-\sqrt{1-u^2}\right)-1\right) \tag{s9}$$

The extremum values of the energy are reached when:

$$\frac{\partial E_2}{\partial n} = \frac{\partial E_2}{\partial u} = \frac{\partial E_2}{\partial v} = \frac{\partial E_2}{\partial B} = 0 \tag{s10}$$

We find that these four equations lead to two sets of solutions, only one of which is a local minimum of the energy function. Choosing the model parameters described in the text, i.e. $\kappa = 8.10^{-19}$ J, $\lambda = 2.10^{-12}$ J.m^{-1}, $\gamma = 5.10^{-4}$ J.m^{-2}, $R_{sp} = 80$ nm, $R_b = 1$ μm and $p = 10^3$ Pa, we find that the interface patterning consists of $n \approx 2400$ domains, which have a radius of curvature $R_c \approx 90$ nm and intersect the bubble with a radius $a \approx 40$ nm (figs. S4 and S5). We conclude from these estimates that the volume of the bubble only

decreases by 6% during the structuring of the interface, with $R_b' \approx 0.98$ μm.

Stability of the microbubbles

The shrinkage of bubbles is due to the diffusion of air in the bulk phase, driven by Laplace pressure. The arrested or significantly reduced dissolution can be rationalized by a decrease in mass transfer to the bulk phase or in driving force, i.e. pressure inside the bubble.

Limited permeability: The permeability or average speed of transport (representative of a flux) quantifies the diffusion of gas molecules through a layer of molecules of characteristic thickness (surfactant or bulk molecules) and enables the comparison between these two potential diffusion barriers. The permeability of a monolayer of condensed surfactant molecules has been measured experimentally and is expected to be about 10^{-2}-10^{-3} cm.s^{-1} (*S6*). The permeability of the glucose syrup around a bubble of radius $R_b = 1\,\mu\text{m}$ is defined as the average speed of transport through a layer of thickness R_b: D/R_b. D is estimated using the Stokes-Einstein relation: $D = \frac{k_B T}{6\pi\eta l_o} \approx 10^{-9}$ cm^2.s^{-1} where η is the viscosity of the glucose syrup (22 kg.m^{-1}.s^{-1}) and l_o the radius of a gas molecule (0.1 nm). The permeability is about 10^{-5} cm.s^{-1}. The layer of glucose syrup has the lowest permeability and sets the rate of diffusion.

Using the Epstein-Plesset model (*S7*) and assuming that the diffusion is driven by Laplace pressure, the dissolution time can be estimated as:

$$t_D \approx \frac{{R_b}^2}{3Dk_H}\left(\frac{R_b\rho}{2M\gamma}\right) \approx 5 \text{ hours} \qquad \text{(s11)}$$

where k_H is the Henry's law coefficient, which is taken equal to that for one of water, assuming that the air solubility is the same in these aqueous phases (8.10^{-6} mol.m^{-3}.Pa^{-1}), ρ the density of air (1.2 kg.m^{-3}), M the molecular weight of air (29 g.mol^{-1}) and γ the surface tension (5.10^{-4} J.m^{-2}).

Inner pressure and elasticity of the surfactant layer: The shrinkage of the bubble leads to interfacial compression, which is opposed by the bending elasticity of the domains. Prior to shrinkage, the reference state of the bubble of radius R_b is defined using the energy minimization approach described above, at almost constant radius, which consists in determining the number of domains, n, and their geometry (a, R_c). Upon limited compression, we can assume that the individual surface area (A) and the number (n) of the domains remain equal to their initial values. When the bubble radius decreases to a value R, the domains are modeled with spherical caps of radius a' and radius of curvature R_c':

$$a' = \frac{2R}{\sqrt{n}} \qquad {R_c}' = \frac{R_b}{\sqrt{n}} \frac{1}{\sqrt{1-\left(\frac{R}{R_b}\right)^2}} \qquad \text{(s12)}$$

The shrinkage is arrested when the work of the Laplace pressure, $\int pdV$, is equal to the change in bending energy of the monolayer from the reference state. The Laplace pressure is due to the presence of narrow regions or boundaries *between* domains where

surfactant molecules are expected to be in liquid state: $p = \gamma\left(\frac{1}{R_1} + \frac{1}{R_2}\right)$, R_1 is the radius of curvature along the boundary, equal to the radius of the bubble, and R_2 the radius of curvature across the boundary, which is negative. The Laplace pressure is overestimated with $p = \frac{\gamma}{R}$, where R is the radius of the bubble.

The arrested state is defined by the following relation:

$$\left| \int_{R_b}^{R} \frac{\gamma}{x} 4\pi x^2 dx \right| - 2nA\kappa \left[\left(\frac{1}{R_c^{'}} - \frac{1}{R_{sp}} \right)^2 - \left(\frac{1}{R_c} - \frac{1}{R_{sp}} \right)^2 \right] = 0 \qquad \text{(s13)}$$

where κ and R_{sp} are the bending rigidity and the spontaneous radius of curvature of the monolayer. nA is equal to the constant surface area of the bubble ($4\pi R_b^2$). This equality is verified by $\frac{R}{R_b} \approx 0.94$ which is the physical solution and is associated to the following domain geometry $a^{'} \approx 38\,\text{nm}$ and $R_c^{'} \approx 60\,\text{nm}$. According to this calculation, the shrinkage should be arrested early on, after a decrease in bubble radius of about 6%.

References and Notes

S1. S. Brockbank, *Surfactant Stabilized Gas Microcells* (PhD thesis, University of Bristol, 1997).

S2. J. N. Israelachvili, *Intermolecular and Surface Forces* (Academic Press, New York, 1992).

S3. G. Garofalakis, B. S. Murray, *Langmuir* **18**, 4765 (2002).

S4. Y.K. Li, S. F. Zhang, Q. H. Wang, J. Z. Yang, *Tenside Surfactants Detergents* **41**, 26 (2004).

S5. B. M. Ocko *et al.*, Phys. Rev. E **55**, 3164 (1997).

S6. M. A. Borden, M. L. Longo, *J. Phys. Chem. B* **108**, 6009 (2004).

S7. P. B. Duncan, D. Needham, *Langmuir* **20**, 2567 (2004).

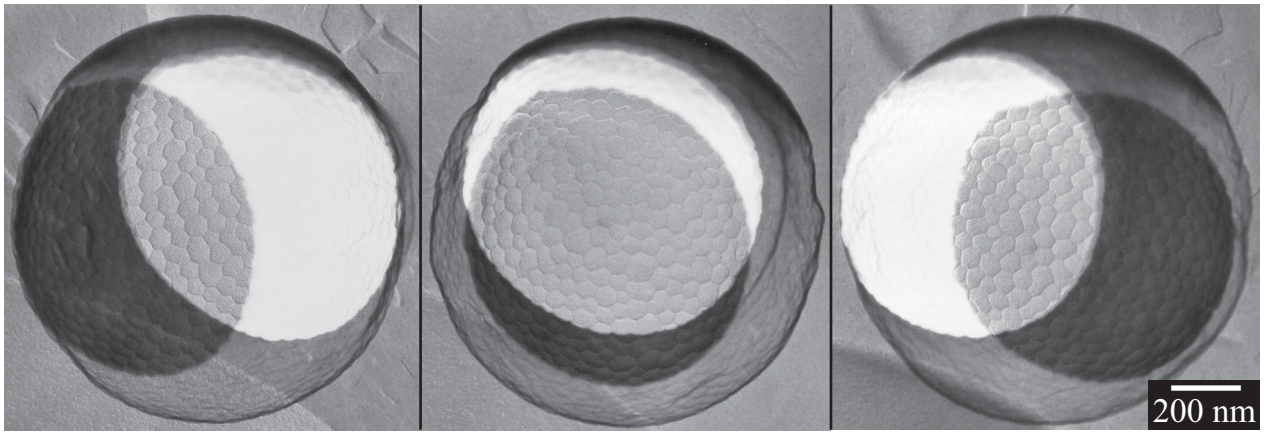

Fig. S1. Evidence for the hollowness of the microbubbles. The freeze fracture replica of a micrometer size bubble is imaged by TEM. Each image corresponds to a given angle between the sample plane and the electron beam. Rotating the replica leads to a shift in the position of the shadowed area.

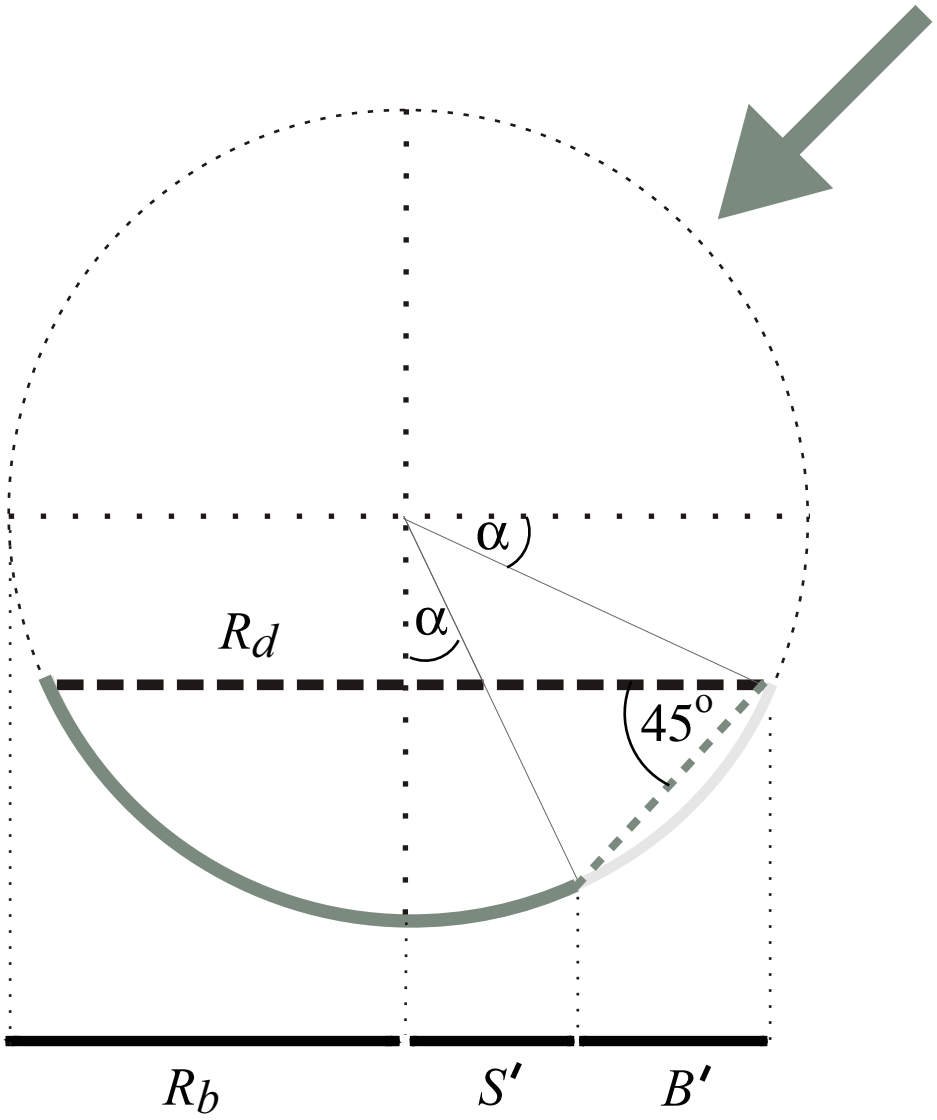

Fig. S2. Radius of the microbubble. During the preparation of the replica, the sample is fractured along a plane that intersects the bubble of radius R_b, leading to the formation of a spherical cap with a base radius R_d. This spherical cap is shadowed with platinum under an angle of 45° (as indicated by the dark grey arrow). Only part of the spherical cap is covered with platinum (represented here in solid dark grey). The angle α is equal to $\arcsin(S'/R_b)$.

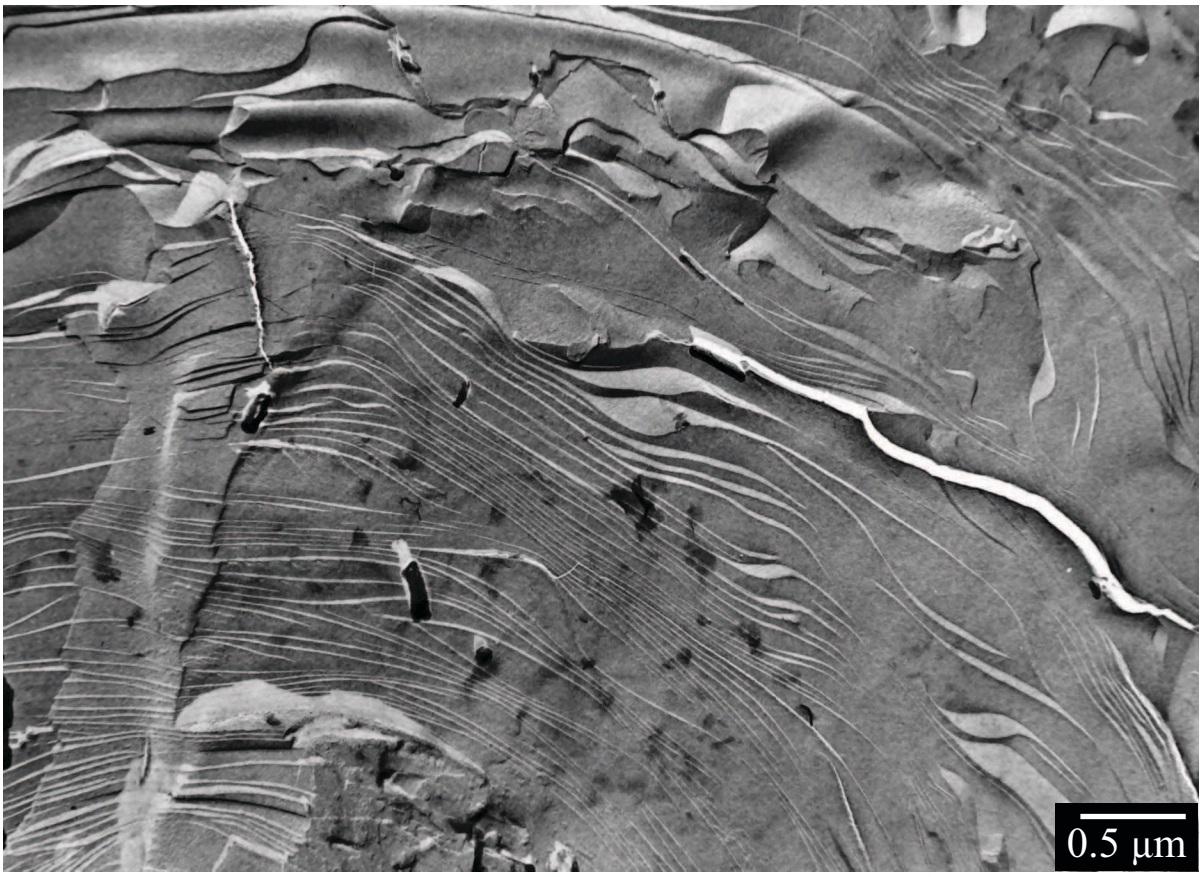

Fig. S3. Lamellar phase before aeration of the surfactant mixture. Before aeration, the mixture of glucose syrup (70% wt. %), sucrose esters (2 wt. %, S1670) and water shows lamellae, which correspond to the condensed phase of surfactant molecules (S1). The regular structure of the lamellae can be differentiate from the cracks (wide, white fractures of the replica) and the debris (isolated dark pieces of material with projected white shadows).

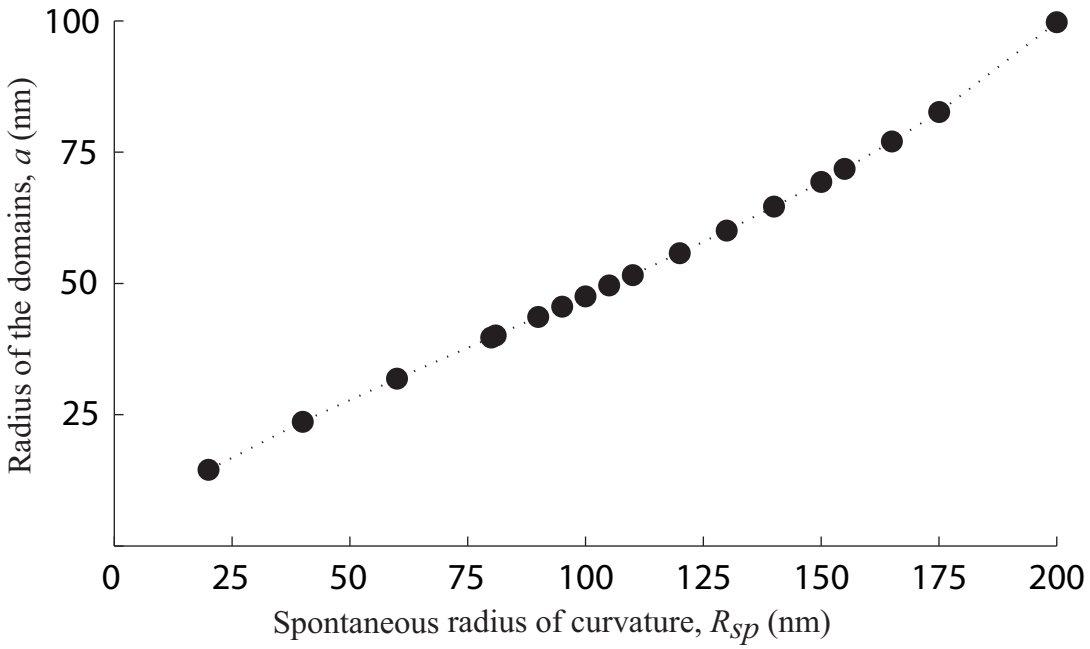

Fig. S4. Prediction from the thermodynamic model for the dependence of the pattern radius on the spontaneous radius of curvature. The pattern radius, a, is an increasing function of the spontaneous radius of curvature of the surfactant monolayer, R_{sp}.

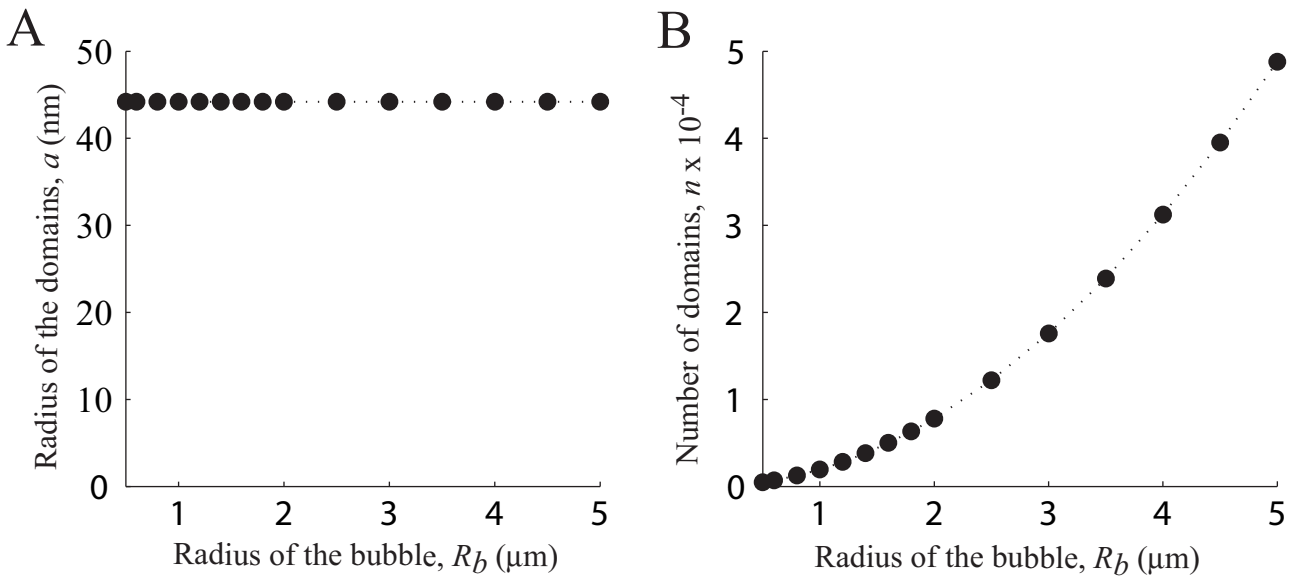

Fig. S5. Prediction from the thermodynamic model for the dependence of the pattern strcuture on the radius of the bubble. (**A**) The pattern radius (a) does not show a significant evolution while the bubble radius, R_b, increases from $0.5\,\text{to}\,5\,\mu\text{m}$. (**B**) The number of domains however is an increasing function of the radius of the bubble.